Photoelectron Spectroscopy of Cuprate Superconductors

David W. Lynch and Clifford G. Olson

Department of Physics and Astronomy and Ames Laboratory, USDOE,

Iowa State University, Ames IA 50011

Abstract

We present a review of the current status of angle-resolved photoelectron spectroscopy of the valence bands of cuprate superconductors, including results from the first half of 1996.

1 Introduction

Photoelectron spectroscopy has contributed significantly to our understanding of the electronic structure of cuprate superconductors in both their normal and superconducting states. In the following, we review the information achieved by the technique of angle-resolved ultraviolet valence-band photoelectron spectroscopy (ARUPS). Some of the most definitive studies have been carried out on $Bi_2Sr_2CaCu_2O_8$ (Bi2212) because its surfaces are more predictable and stable than those of other cuprates. Extensive ARUPS studies have been carried out on $YBa_2Cu_3O_7$ (Y123), which has been more widely studied than Bi2212 by all other physical techniques. Studies have been extended to other members of the Bi2212 and Y123 families, as well as to the $Nd_xCe_{2-x}CuO_4$ and the oxy-chloride systems. As "better" single crystals of other cuprates become available it is certain that extensive ARUPS studies will be made without delay. Some of the important questions photoelectron spectroscopy can address, but usually not answer in a simple direct way, are the nature of the normal state (Fermi liquid or not), wave vector dependence of the energy of the photoexcitations (hole quasiparticles) and sometimes their symmetry, the effects of doping on the electronic structure, and the magnitude, anisotropy, and temperature dependence of the superconducting order parameter. Such studies were not carried out on traditional superconductors because the states of interest are within a few k_BT_c of the Fermi energy, a region too narrow for study by photoelectron spectroscopy. The cuprates had values of

T_c so much larger that resolution improvements made their study feasible.

In the following, we outline briefly experimental techniques, emphasizing present limits on resolution and samples. This is followed by a brief description of the theoretical basis for photoelectron spectroscopy. Good reviews of photoelectron spectroscopy exist (Cardona and Ley, 1978; Ley and Cardona, 1979; Plummer and Eberhardt, 1982; Smith and Himpsel, 1982; Courths and Hüfner, 1984; Kevan, 1992; Hüfner, 1995). The bulk of the paper describes experimental results to date. Some of these have implications for microscopic models of the electronic structures of the cuprates, both in the normal and superconducting states. Detailed interpretation of all aspects of the spectra requires a microscopic model, but at the time of this writing, there is not universal agreement on such models. For this reason, and for lack of space, we do not discuss some of the possible interpretations of the data.

There is an enormous literature on cuprates, and a very large one on photoelectron spectroscopic studies on them. To keep the length of this review manageable we concentrate almost exclusively on ARUPS. Angle-integrated photoelectron studies of valence bands, and the study of core level spectra are mentioned only briefly to justify an occasional statement. Similarly, we cannot reference all ARUPS work, but refer the reader to several reviews (Lindberg et al., 1990; Brenig, 1995; Shen and Dessau, 1995; Lynch and Olson, 1997). Results from photoelectron spectroscopy should not be studied in isolation. There are many related spectroscopies whose results should be melded with those of photoelectron spectroscopy. These include x-ray absorption and emission, and electron energy loss spectroscopies. These have been reviewed elsewhere (Fink et al., 1994; Bozovic and van der Marel, 1996). It is also useful to compare photoelectron spectra of the cuprates with those of related materials, e.g., CuO and NiO, but there is not space in this short review to do so. An excellent review of the electronic structure of 3d-transition-metal oxides exists (Hüfner, 1994).

2 Experimental aspects of angle-resolved photoelectron spectroscopy

Conceptually the experiment is simple. A photon excites an electron in a many-electron system. Ideally it emerges from the sample with no measurable change in energy or direction due to internal scattering processes, and it is detected by an angle-resolving electron energy analyzer. From its measured energy and direction, its wave vector is determined. The component of this wave vector normal to the surface has been altered upon escape by the potential "step" at the surface, but for a "good" surface, the parallel component is conserved, modulo a surface

reciprocal lattice vector. (The other component of **k** sometimes may be obtained through further measurements, but for two-dimensional materials like Bi2212 it is not necessary. Y123 is not adequately two dimensional). Use of the photon energy $h\nu$ and the kinetic energy of a Fermi level electron from a reference metal gives the initial state of the electron (or system - see below) E_i, and, since the photon wave vector is small on the scale of electron wave vectors, the initial-state wave vector is the same as that of the final state, modulo a reciprocal lattice vector.

Because work functions range up to about 5 eV or so, energetic photons are required. The commonest sources are the He I and He II lines at 21.2 and 40.8 eV respectively, and synchrotron radiation dispersed by a monochromator. The latter has the advantage of selectable photon energy, allowing use of the energy dependence of the photoexcitation cross section to select for or against particular subshells of electrons. With current technology, the best resolution achieved to date is about an 8 meV spectral bandpass from a monochromator and 5 meV resolution in electron energy analysis. Taking the square root of the sum of the squares gives an overall resolution of about 10 meV. Most of the work reported below used an overall resolution of 25 meV or larger. The best angular acceptance used to date for studies on cuprates is about 1°. This translates into an uncertainty in the parallel component of the wave vector and in the case of dispersive states degrades the energy resolution.

Photon energy resolution may be limited by aberrations in the monochromator, and electron energy resolution by stray electric or magnetic fields or geometric imperfections in the analyzer. When none of these is the limiting factor, then the acceptable flux imposes a limit. Improving resolution always means reducing the flux of photons on the sample. If the flux is reduced, the time to obtain a spectrum at constant signal to noise ratio increases. If surfaces are not stable for long periods of time, the spectra must be taken quickly. In any case, studies on cuprates require many spectra to be taken, and even with stable surfaces and high-quality vacuum, time is always a factor. In the near future, there will be several new beam lines in operation that should yield overall resolutions of 7-8 meV with angular resolution of about 0.5°. Further improvement appears possible.

ARUPS is very surface sensitive. The mean free path for escape without inelastic scattering is only of the order of 10 Å, i.e., only about a third of the unit cell height for Bi2212. ARUPS requires single crystals. Surfaces must be prepared and measured in ultrahigh vacuum, pressures in the range of 10^{-10} Torr or below. For cuprates, this has traditionally be done by cleaving. The sample is epoxied to a post, and a tab or another post epoxied on top. In vacuum, the upper post is knocked off, giving a cleavage surface. Some of these surfaces have been adequate for ARUPS studies of several cuprates, but for others, e.g., $Tl_2Ba_2CuO_6$, the surface quality has been poor and no ARUPS peaks have yet been found.

Early work on Eu123 (List et al., 1988) showed that spectra measured at 20 K on a surface cleaved at 20 K, then warmed to about 100 K for a few minutes, then recooled to 20 K showed an irreversible change. This was consistent with the loss of a small amount of oxygen to the vacuum, an effect later used to explain LEED observations of reconstructed Y123 surfaces (Behner et al., 1992) and with the STM observations of Edwards et al. (1992) Since then, nearly all ARUPS studies have used surfaces cleaved at 20 K and held there, except for temperature increases of short duration to take data above T_c.

The quality of the surface is very important. Differences in the results of several groups, especially in the early years, are most likely due to differences in the quality of the sample surfaces, which derive from the quality of the single crystals used. It has not been easy to determine what plane is exposed upon cleaving. Core-level studies by x-ray-induced photoelectron spectroscopy have been used to try to determine this, but the situation is complex. For example, these studies show that Bi2212 cleavage surfaces are Bi–O planes. It is believed the cleave occurs between pairs of adjacent weakly bonded Bi–O planes and both new surfaces are equivalent. STM studies also show this surface. Such is not the case with Y123, where freshly cleaved surfaces are usually said to be Ba–O planes. From Fig. 1 we see that cleaving between Ba–O and Cu–O planes can be done two ways, along dashed planes marked 1 and 2. Only one of these leaves a Ba–O plane for the surface of the bottom half; the Ba–O plane after cleavage 2 falls away. Cleaves 3 and 4 separate a Ba–O plane from a Cu–O chain. Surfaces 3 and 1, both Ba–O surfaces, are not equivalent because different planes lie below them. If cleaves of the type 1 and 2 are easier, the surface may contain a distribution of them, roughly half the area being a Ba-O surface, with numerous steps. In general, up to four different surfaces could be exposed upon cleaving. There is even a suggestion that in some unusual cleaves an Y surface may be exposed (Schroeder et al., 1993). One way to determine the cleavage surface is to compare photoelectron spectra with those calculated for all possible terminating planes (Calandra and Manghi, 1992, 1994). Bansil et al. (1992) carried out such a calculation of the ARUPS spectra expected for all six possible (1 0 0) surfaces after cleaving. Comparison with experimental spectra led them to conclude that the surface measured was a Ba–O plane with a Cu–O_2 plane just below it. However, Edwards et al. (1992), cleaved surfaces of Y123 in ultrahigh vacuum at low temperature. They observed by STM the cleavage plane to be between a Ba–O plane and the plane of the Cu–O chains. This surface lost oxygen upon being heated to 70 K. (Y123 crystals are also twinned, altering their apparent symmetry. They can be "detwinned", but the breakage rate is very high.)

In addition to the primary photoelectron spectrum, there are secondary electrons, electrons which have lost a measurable amount of energy before escaping (in

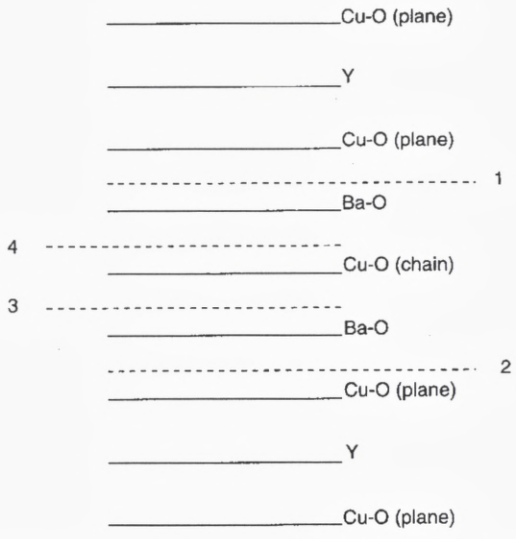

Figure 1. Schematic of the atomic layers in Y123. The numbered dashed lines indicate possible cleaves. See text.

one model of photoemission). These form a nearly structureless background spectrum at kinetic energies lower than those of the primaries, i.e., at greater apparent binding energies. It would be useful to strip this from the measured spectrum, but this has rarely been attempted in ARUPS for several reasons. The inelastic scattering is usually assumed to be due to electron–electron scattering, and for electrons of relatively low energy, any single-scattering model should not be accurate. The electron wavelength exceeds the distance between scattering centers and a multiple scattering formalism should be used. Also, the methods used to remove inelastic backgrounds from XPS spectra require either a part of the spectrum where no primaries are expected to exist or electron energy loss spectra for the material. High-resolution ARUPS scans take considerable time and rarely extend far enough to reach the region of excitation below the bottom of the valence band, and the requisite electron energy loss measurements as a function of both energy and momentum with adequate energy resolution do not exist.

A striking feature of ARUPS spectra of cuprates compared with spectra of other materials is the very large "background". The peaks near the Fermi energy in Bi2212 ARUPS spectra are only about twice as large as the background 300–500 meV below the Fermi energy. This ratio is about the same for spectra taken by several groups on crystals grown by several groups over a period of 7 years. Figure 2 shows spectra taken under comparable conditions for Bi2212 and $TiSe_2$, illus-

trating the difference in apparent backgrounds. Over the past 7 years, the visual quality of the cleaved surfaces has improved, but the background has not changed. One interpretation of this is that for the cuprates this is not a background of inelastically scattered electrons but rather an intrinsic feature of the photoelectron spectrum due to leaving the system in a continuum of excited states (see below). Another is that the surface is intrinsically defective due to the oxygen vacancies introduced by doping to produce the metallic superconductor from the insulating parent compound. Defects spaced an average distance Λ apart can create a wave vector uncertainty of the order of Λ^{-1}. Kevan (1986) has shown that the addition of 1–2% of a monolayer of K atoms to a Cu surface had a broadening effect on the photoelectron spectrum from a surface state. (The inelastic background was not studied). The expected oxygen vacancy concentration in an optimally doped cuprate is comparable to that in Kevan's work. However, there is yet no experimental proof for the origin of the large background found in cuprate spectra. Figure 2 also illustrates how weak a feature one is dealing with in studying the near-Fermi edge photoemission in cuprates. Under comparable conditions, the count rate for the $TiTe_2$ spectrum is about 20 times that of the Bi2212 spectrum. At larger binding energies, the count rate for Bi2212 increases considerably, but this region is of less interest.

3 Theoretical aspects of angle-resolved photoelectron spectroscopy

Although a "three-step" model (excite, transport to the surface, escape) has been used for many years, and is still in use for some purposes, the correct picture is of a one-step process. Initially one has an N-electron system and a photon (which can be treated classically), and at the end, there is an $N-1$ electron system, an electron in the detector, and no photon. The $N-1$ electron system need not be left in its own ground state. The Hamiltonians for the two systems are thus not the same, although if the independent-electron approximation is made, as in band theory, they are the same, and the energy of any one eigenstate is independent of the occupancy of other eigenstates. The energy and momentum of the detected electron are then related to the energy and momentum of the hole in the $N-1$ electron system. The interaction of an electron with the electromagnetic field is effected by the perturbation Hamiltonian, $H' = (e/mc)(\mathbf{A} \cdot \mathbf{p} + \mathbf{p} \cdot \mathbf{A})$, where $\mathbf{A}$ and $\mathbf{p}$ are the vector potential and momentum operators, respectively. The interactions with the surface and with the other electrons (inelastic scattering) are handled in the Green's function G of the final state electron. The photocurrent in the detector is proportional to the product of the square of the electric dipole

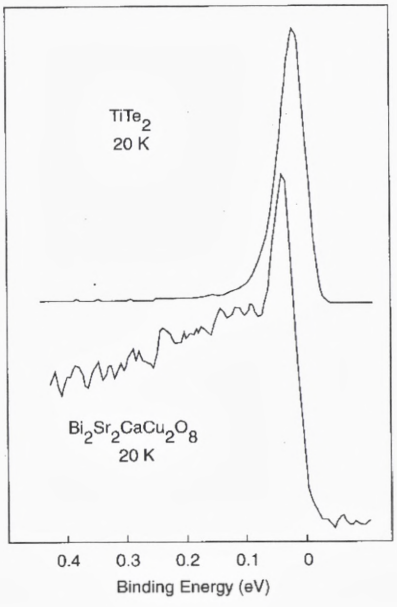

Figure 2. Photoelectron spectra of Bi2212 and $TiTe_2$. These spectra were taken at comparable energy and angle resolutions and photon fluxes. The peak count rate for $TiTe_2$ is about 20 times that of Bi2212. The rising edge in the Bi2212 spectrum is shifted away from the Fermi level because the sample is superconducting.

(momentum) matrix element between initial and final states and the spectral density $A(E, \mathbf{k}) = (1/\pi)\mathrm{Im}G(E, \mathbf{k})$. For negative energies $A(E, \mathbf{k})$ is the spectrum for electron removal, as in photoemission, and for positive E, the spectrum for electron addition, as in inverse photoemission. The proportionality between photocurrent and $A(E, \mathbf{k})$ is valid only if the sudden approximation is valid, and a priori, one does not know above what final state energy this is a good approximation for a given system. Since the early photoemission studies it has been assumed to be valid for valence band electrons photoexcited with 15–25 eV photons. Recently Randeria et al. (1995) put to rest the fears of those concerned by showing that for Bi2212 the sudden approximation was indeed valid for such spectra, a result presumably extendible to all cuprates.

The widths of the peaks in the photoelectron spectra often are interpreted as arising from the lifetime of the photoelectron and photohole, after the removal of instrumental broadening. In a strictly two-dimensional system, the photoelectron lifetime contribution drops out. The photohole width, if its energy dependence can be measured close enough to E_F, would give an important test for many-

body models for the quasiparticles. Unfortunately, the reliable extraction of the photohole lifetime from data is very difficult (Smith et al., 1993). Moreover, Y123 probably is not sufficiently two dimensional to allow such extraction.

4 Early results

Many of the earliest photoelectron studies on cuprates, primarily Y123, were aimed at demonstrating the presence of Cu^{3+} due to the hole doping but these were not very successful. Often the samples were pressed sintered pellets and fresh surfaces were prepared *in situ* by scraping, which may have exposed intergranular material. All work was at room temperature, except for unsuccessful attempts by UPS to detect the opening of a gap. Photoelectron spectra of the valence bands in these samples rarely showed a Fermi edge, although the bulk samples were known to be metallic. The angle-integrated valence-band photoelectron spectra often resembled those from LDA calculations, but the few features often were shifted to greater binding energy, and there was an unexpected peak at around 9 eV binding energy. Both of these are now believed to be due to the effect of the loss of oxygen to the vacuum, making the surfaces somewhat insulating so they become charged positively upon photoemission. The 9 eV peak is now taken as the signature of a deteriorated surface.

Attempts to see a gap open up upon entering the superconducting phase eventually were successful (Olson et al., 1989). These required single crystal samples cleaved at low temperatures. Bi2212 was the sample of choice, for its cleaved surfaces were much more stable in vacuum than those of Y123, and they could be studied even at room temperature. This early work, at 28–32 meV overall resolution, established a number features of the ARUPS spectra. A peak was tracked from below the Fermi surface till it crossed the Fermi surface along the ΓX line at the wave vector predicted by LDA calculations. (The Brillouin zone is shown in Fig. 4, which illustrates more recent data.) The effective mass was about twice that of the LDA calculation. There seemed to be no effect of the superlattice along the b-direction, but better crystals later showed this result to be spurious. The bands just below E_F along the $\Gamma\bar{M}$ line were rather complicated and not resolved. Finally, the width of the peak along ΓX, decidedly non-Lorentzian, depended strongly on binding energy, and the dependence was linear, not quadratic. However, the quadratic dependence is expected for a Fermi liquid only in a very limited energy range spanning E_F, and the finite energy and momentum resolution causes an effective integration over a region even wider than that for which the quadratic dependence is expected. Moreover, the extraction of a lifetime width from a measured width is extremely difficult to do reliably (Smith et al., 1993). Finally, upon

cooling below T_c, the photoelectron peak "at" E_F was seen to retreat, not rigidly, with a pileup of intensity at the new edge. Fitting to a BCS model gave a gap energy Δ of about 20 meV. There are now different and better ways to extract the gap from the data. The value of 20 meV is probably still correct to within 5 meV, but it represents only the maximum gap at 20 K. This gap was found originally not to depend on wave vector in the basal plane, but more recent work finds considerable anisotropy in good samples. More extensive recent work with improved samples and improved resolution by several groups has confirmed a number of these features, and found many new features. Crystals grown more recently have given some results that are different from those just described. These crystals presumably have better crystallinity and homogeneity. (However the background described above is not smaller).

Similar early work on Y123 also established that the LDA Fermi surface was close to the experimental one, although one part of it was not seen in the experiment. The Fermi edge was weaker than in Bi2212, and no reliable estimates of the gap were published.

5 Current status

Most work has been done on samples near optimal doping. This will be assumed in the following, unless stated otherwise. Photon energies in the 15–25 eV range are usually used because of the broad maximum in the O $2p$ photoexcitation cross section. The structures of interest have widths comparable to the best resolution used to date. The intrinsic spectral shapes then appear in the measured spectra only after convolution with the instrument function, which depends on energy and angle. Assuming these can be factored, the energy part can be determined by measuring the Fermi edge on metal like Pt. The angle dependence is normally not known, and a Gaussian is substituted with a width given by the nominal angular acceptance of the analyzer. Absolute line shapes, or parameters in an assumed line shape are thus not very precisely known. Many conclusions can be drawn without such precise knowledge, however. More important is whether the spectra have been reproduced by at least two groups.

5.1 Bi2212

Band mapping has been carried out in the normal state. Because of the complexity of the bands, only the first 0.5 eV below the Fermi energy has been studied intensely. Earlier work mapped a number of deeper valence bands, but identification with theoretical band structure was difficult. There was initial disagreement in the results of different groups even in the number of bands observed crossing the Fermi

level along a line in reciprocal space. This probably was the result of actual sample differences, both the bulk samples and in the quality of the cleaved surfaces. Figure 3 shows a series of typical scans such as now have been recorded by several groups. One can see a peak that disperses with wave vector, passing through the Fermi level and disappearing. This gives one point on the Fermi surface. Such scans have been carried out for wave vectors covering the ΓXY plane of the Brillouin zone to produce a Fermi surface in good agreement with that from LDA band calculations (Fig. 4). Spectra with peaks below E_F are used to map the quasiparticle band. Along some regions of the Brillouin zone, e.g., ΓX, the experimental band is close to parabolic, but its effective mass is about twice that of the LDA calculation. Along $\Gamma\bar{M}$ the bands are more complex, running rather parallel to the surface. By scanning perpendicular to the $\Gamma\bar{M}$ line along lines passing through this flat region, a line of critical points (near critical points, if we consider experimental resolution), saddle points, has been found. This is a persistent feature, found in many cuprate superconductors.

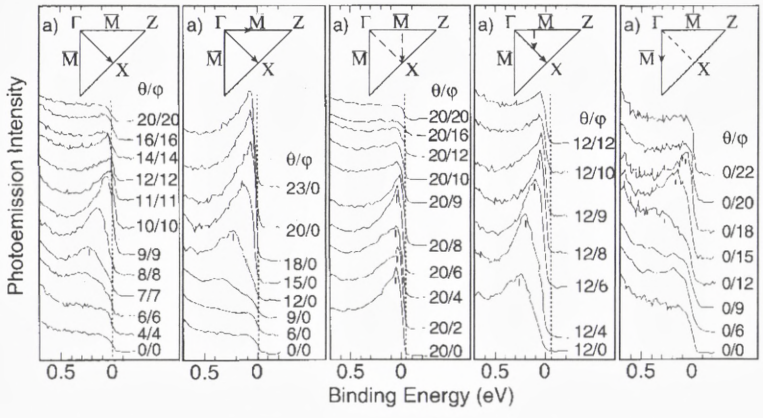

Figure 3. ARUPS scans on Bi2212 at 100 K. The locations of the points in reciprocal space are marked in Fig. 4. (Dessau et al., 1993).

The ΓX and ΓY lines should be nearly equivalent, for the a and b lattice parameters are nearly the same. However, they are not nearly equivalent. There is a superlattice with a repeat distance along the b axis of about 27 Å. The new orthorhombic unit cell is approximately a $\sqrt{2} \times 5\sqrt{2} - 45°$ cell in the tetragonal lattice, a larger unit cell with a smaller Brillouin zone. The bands remap and

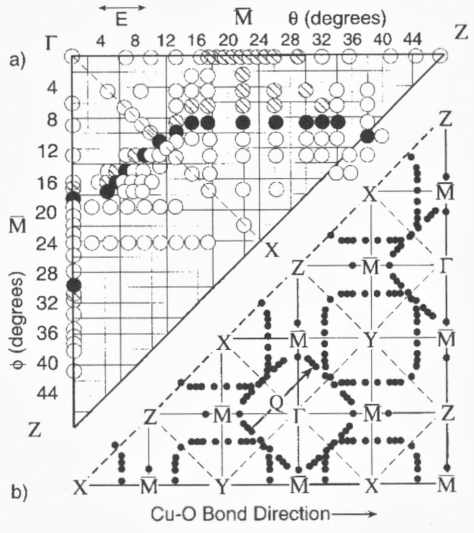

Figure 4. (a) Fermi surface of Bi2212 marked by filled circles. The points where a band crosses E_F were determined from the data in Fig. 3. Empty circles mark locations in the Brillouin zone with no states observed at E_F. Shaded circles mark spectra with states at E_F that do not clearly pass through it in nearby scans. The circle diameters indicate angle resolution. (b) The Fermi surface of (a) repeated in the extended zone by the use of symmetry. **Q** denotes a nesting wave vector. (Dessau et al., 1993).

gaps open at band crossings. Singh and Pickett (1995) have calculated the effect of a similar reconstruction in Bi2201 on the LDA band structure and find rather large effects. Bands based on Bi–O states (the Bi–O planes distort the most in the reconstruction) shift up to 0.4 eV and the Fermi surface is altered. Still, to date, most ARUPS data on Bi2212 are compared with the results calculated for a tetragonal, not orthorhombic, unit cell.

Aebi et al. (1994, 1995) and Osterwalder et al. (1995) measured the photocurrent originating from the Fermi level of Bi2212 over a very fine mesh in angle, taking several thousand spectra over almost 2π steradians. This was done at 300 K. They also examined a Pb-doped sample for which the superlattice does not occur. In addition to the previously known Fermi surface, they found some parts of the Fermi surface exhibiting two-fold symmetry which gave weak signals not present in the Pb-doped samples, see Fig. 5. These were attributed to the effect of the superlattice. They also found several sets of weak "shadow bands" crossing the Fermi surface. These were attributed to antiferromagnetic correlations, rather than Umklapp processes. Kelley et al. (1993) reported differences in dispersion

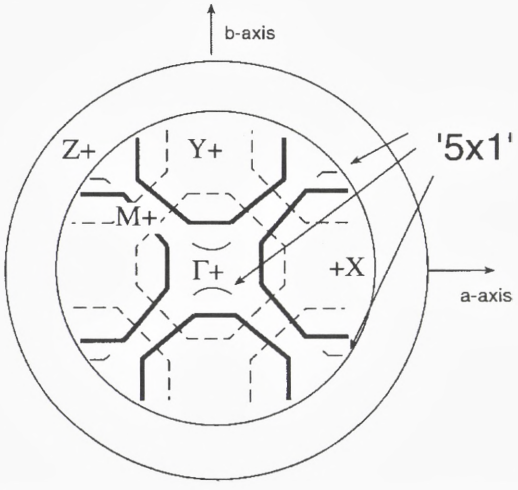

Figure 5. Stereographic projection of the Fermi surface of Bi2212 obtained by Osterwalder et al. (1995). The heavy lines mark the trace of large photocurrents from the normal Fermi surface, as in Fig. 4. The dashed lines are the weaker "shadow bands". The small arcs marked 5×1 result from the superlattice. The outer ring of the stereogram represents photoemission parallel to the surface.

between the band crossing E_F along ΓX and along ΓY due to the superlattice. The superlattice and shadow bands were also studied by Ding et al. (1996).

Bi2212 contains two pairs of Cu–O_2 planes, each of which contributes a degenerate set of bands near E_F. Weak interaction between these planes should produce bonding-antibonding pairs of bands, but this has not been found (Ding et al., 1996a) in one recent set of measurements. LDA calculations indicate a splitting of about 0.25 eV near the $\bar{M}$ point (Massida et al., 1988) which would be reduced by many-body effects. Liechtenstein et al. (1996) showed that many body effects reduced the LDA splitting from 300 meV to 40 meV in a model calculation. Depending on dipole matrix elements, a 40 meV splitting might or might not be expected to have been detected in the data Ding et al. took at 13 K.

The ARUPS band maps all indicated a flat band just below E_F along the $\Gamma\bar{M}$ direction. Such a flat region has been found in many cuprates, not just Bi2212, but its distance below E_F varies from material to material, and with doping for any one material. For all the hole-doped cuprates, this flat region is close enough to E_F to be important in any model for the superconductivity.

The original report (Olson et al., 1990) of the photohole lifetime varying as $(E - E_F)^1$ has been controversial, with several discussions of better fitting proce-

dures having appeared subsequently. In fact, it was measured on too coarse an energy scale to related directly to Fermi liquid theory. Moreover, the line shape was not Lorentzian and the width was not small with respect to the photohole energy. At this time, this result remains a tantalizing curiosity. More can be done with higher resolution spectrometers, better knowledge of the final states, and, especially, an understanding of the inelastic background in the ARUPS spectra, if indeed that is what it is.

The first hints of anisotropy in the superconducting order parameter Δ ("the gap") came in 1992 (Wells et al., 1992). The most recent measurements indicate that it has $d_{x^2-y^2}$ symmetry (Shen et al., 1993; Yokoya et al., 1996), see Fig. 6. This has now been found by several groups, and seems to be a secure result. The largest value for Δ, one half the gap, is about 25 meV $\pm$ 5 meV, about 6 $k_B T_c$, and the largest value occurs along the $\Gamma\bar{M}$ line, which corresponds to the direction of the Cu–O bond in real space. The minimum value is 0 with about the same uncertainty, and the minima occur along ΓX and ΓY, 45° from the maxima. (Photoelectron spectra give only the absolute magnitude of the gap). The early determinations of the gap fit the spectral peak in the normal phase to a Lorentzian multiplied by a Fermi-Dirac function convolved with an instrument function. In the superconducting phase, the Lorentzian width was reduced and it was multiplied by the BCS "density of states" although the latter is not appropriate for such a limited volume of reciprocal space. Later work often used the shift of the 50% point on the initial edge near the Fermi energy to obtain Δ. Fehrenbacher (1996) has shown how difficult it is to extract Δ from experimental data with finite energy and angle resolution. The angle dependence of the instrument function is rarely known well.

The temperature dependence of Δ has been measured often, but rarely published because the error bars grow very large as T_c is approached from below. All groups find Δ decreases with increasing T less rapidly than the well-known BCS result $\Delta(T)/\Delta(0) \sim (1-T/T_c)^{1/2}$ near T_c, in accord with strong coupling theories. There is one report (Ma et al., 1995) of a different temperature dependence for different directions in reciprocal space, but this has not been reported by more than one group.

Below T_c in many parts of the Brillouin zone there is a dip at about 90 meV (about 3–4 Δ) below E_F, followed by a peak at about 100 meV (Dessau et al., 1991, 1992), see Fig. 6. This peak is most prominent for spectra taken along directions in the Brillouin zone associated with larger values of Δ, e.g., $\Gamma\bar{M}$, and small or missing where Δ is small, e.g., ΓX. Ding et al. (1996a) indicate that this structure is not the result of two independent peaks with a valley between. The spectral intensity on both sides of the dip varies in the same way as the photon polarization is changed. The current explanation of this dip is that the opening of

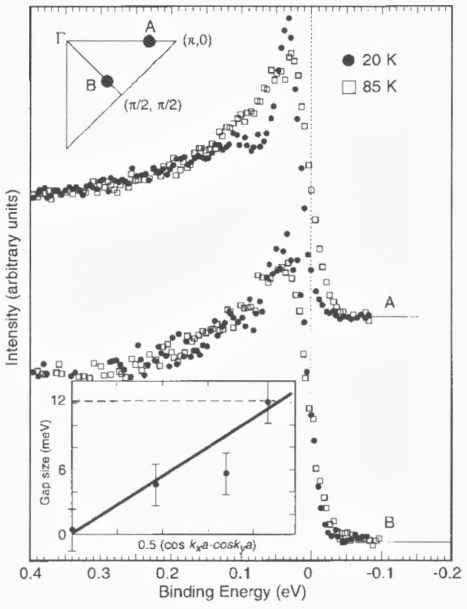

Figure 6. Angle-resolved photoelectron spectra of B12212 below and above T_c at two points in the Brillouin zone, marked in the upper left corner. The shift of the edge and pileup below the edge can be seen in A, where the gap is relatively large. At point B the gap is much smaller. Note also the dip at about 90 meV binding energy for $T < T_c$. The inset shows the dependence of the gap on angular position in the Brillouin zone. (Shen et al., 1995).

a gap suppresses the line width for $E < 3\Delta$, sharpening the structure between 0 and 70 meV (Varma and Littlewood, 1992; Coffey and Coffey, 1993).

Campuzano et al, (1996) recently published an esthetically satisfying study of the approach and retreat of the edge of the Bi2212 ARUPS spectrum. At low temperatures, the BCS spectra function is $A(\mathbf{k},\omega) = (\pi/2)\Gamma(1 - \epsilon_{\mathbf{k}}/E_{\mathbf{k}})/[(\omega + E_{\mathbf{k}})^2 + \Gamma^2]$, where $\epsilon_{\mathbf{k}}$ is the normal state energy and $E_{\mathbf{k}} = (\epsilon_{\mathbf{k}}^2 + |\Delta(\mathbf{k})|^2)^{1/2}$ is the quasiparticle energy, both measured from E_F. Γ is a line width. The normal state spectrum results if $\Delta = 0$, and any spectral peak, followed as a function of $\mathbf{k}$, should pass through E_F from below and disappear. Below T_c, the closest a peak in $A(\mathbf{k},\omega)$ can come to E_F is Δ. Scanning from below E_F, the peak in $A(\mathbf{k},\omega)$ should follow the curve shown in Fig. 7, approaching E_F, but then retreating from it with decreasing intensity, as the quasiparticle amplitude for these $\mathbf{k}$ values is predominantly above E_F. Such behavior was seen in the spectra of Campuzano et al. (Figs. 8 and 9).

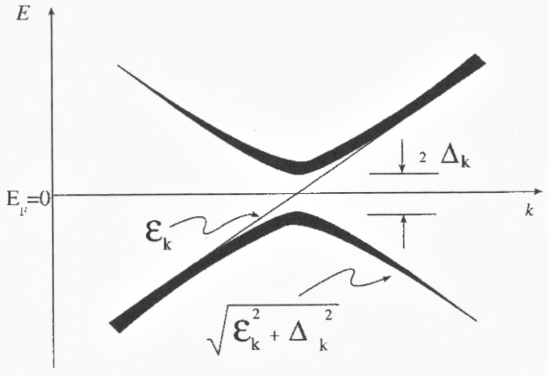

Figure 7. Behaviour of expected quasiparticle dispersion in the normal (thin straight line) and superconducting state. The line width of the lower curve for the superconducting state indicates the intensity expected in the photoelectron spectrum. (Campuzano et al., 1996).

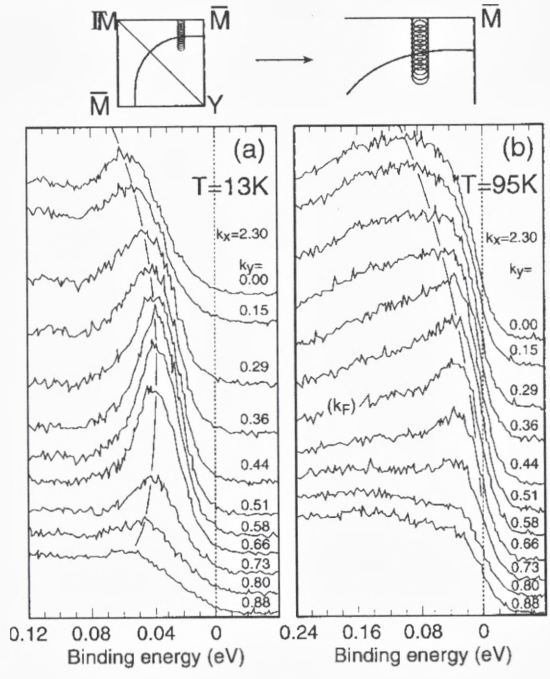

Figure 8. Photoelectron spectra from Bi2212 above and below T_c. The solid curve is a guide to the eye. In the normal state, the curve approaches close to the Fermi level while in the superconducting state, it approaches, then retreats. The wave vectors are in units of $(1/a)$. (Campuzano et al., 1996).

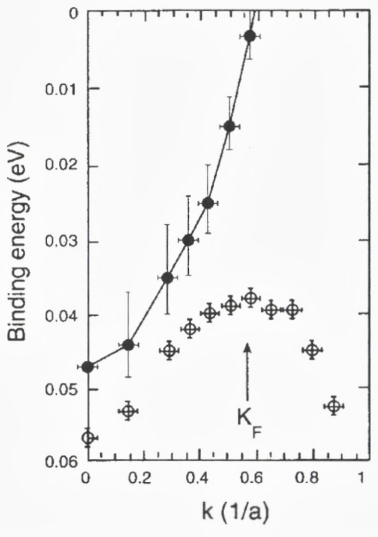

Figure 9. Distribution of maxima in the spectra of Fig. 7, plotted as a dispersion curve. Solid points: normal state; open points: superconducting state. Compare with Fig. 7. (Campuzano et al., 1996).

Photoemission studies on underdoped Bi2212 samples with lower values of T_c recently revealed a surprise (Marshall et al., 1996; Loeser et al., 1996; Ding et al., 1996b). Above T_c, parts of the Fermi surface were missing. It was suggested that this was the result of the opening of a gap, even at $T > T_c$. A gap with $d_{x^2-y^2}$ symmetry was then found. There are several possibilities for the origin of this gap. That the sample was no longer superconducting could be attributed to the lack of long-range coherence in the system of pairs (Emery and Kivelson, 1995).

5.2 Y123

Band mapping of Y123 has been carried out less frequently. Crystals cleaved at low temperature, then warmed above T_c often are not stable, though different groups have reported that some samples or cleaves are more stable than others. Band mapping can be carried out below T_c, however (Tobin et al., 1992; Liu et al., 1992). The LDA Fermi surface is shown in Fig. 10 along with experimental points from ARUPS . The calculated Fermi surface shown is a projection of the actual three-dimensional surface on the plane normal to the k_z axis, the widths of the shaded regions indicating the degree of k_z dependence of the Fermi surface. The contributions of bands from both the Cu–O chains and the Cu–O planes were

found, and agreement with the LDA calculations appears rather good. Liu et al. varied the oxygen stoichiometry between 6.3 and 6.9 per formula unit and found approximately the same Fermi surface for the two metallic samples. The insulating sample ($x = 6.3$) had a very small Fermi surface. This was an early hint of the difference between metallic and insulating samples in the cuprates. Thinking of cuprates as doped insulators leads to a small Fermi surface, with volume (area) proportional to the number of holes added to the half-full valence band. This is what is suggested in the data of Liu et al., and in the recent work on Bi2212 by Marshall et al. The metallic cuprates have a larger Fermi surface, with volume proportional to the number of electrons in the band, as expected from Luttinger's theorem. Photoemission studies of Y123 have been reviewed by Veal and Gu (1994).

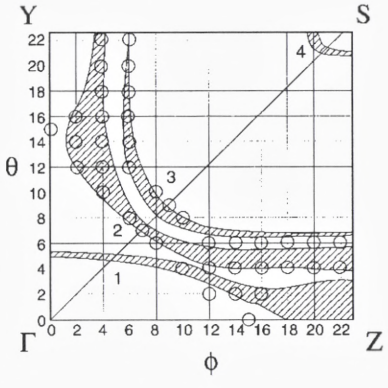

Figure 10. Calculated Fermi "surface" (shaded) and Fermi surface points determined by ARUPS for Y123. The ARUPS data were taken on a twinned single crystal. The points from the Cu–O plane bands have reflection symmetry about the ΓS line. The points from the chain bands do not. (Liu et al., 1992).

Further study (Abrikosov et al., 1993; Gofron et al., 1994) by scanning through the flat band along ΓY just below E_F, but scanning perpendicular to the ΓY line, revealed the presence of a line of saddle points (Figs. 11 and 12). Such an extended saddle point gives a stronger divergence in the density of states than does a simple saddle point.

The Fermi edge is rather weak, and most studies going below T_c did not report a peak, although there have been some reports of a shift of about 20 meV upon going from about 100 to 20 K. All studies reported a very sharp peak at about 1 eV binding energy. This peak, sometimes considered to be from a surface state,

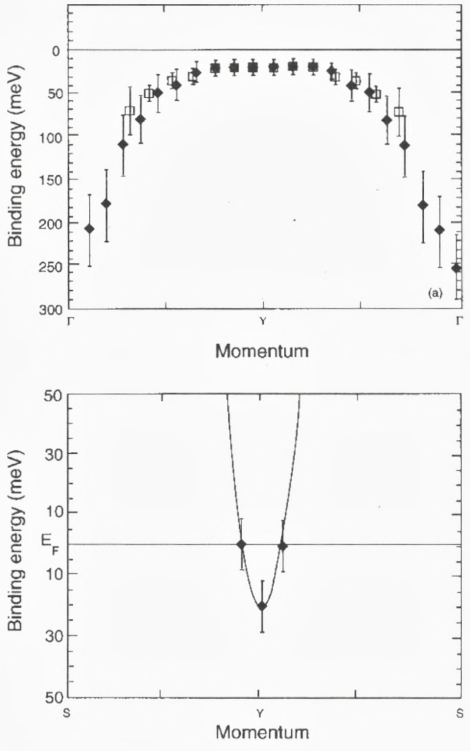

Figure 11. Position of ARUPS peaks from Y123 along the ΓY line in the Brillouin zone and along a line, YS, perpendicular through it, illustrating the extended saddle point. (Abrikosov et al., 1993).

disperses measurably (Tobin et al., 1992). Schroeder et al. (1993) described some "anomalous" cleaves, the surfaces of which had a larger edge at E_F and a smaller peak at 1 eV. These samples showed a clearer edge shift and pileup around E_F when cooled below T_c, leading to an estimate of a gap of about 20 meV.

5.3 n-type cuprates

$Nd_{2-x}Ce_xCuO_4$ goes superconducting with its highest T_c around 25 K for $x = 0.15$. In the normal state the carriers are electrons, not holes. Many of its properties in the normal phase are not "anomalous" like those of the other cuprates whose charge carriers are holes. ARUPS measurements (Sakisaka et al., 1990; King et al., 1993; Anderson et al., 1993) produced a Fermi surface in good agreement with

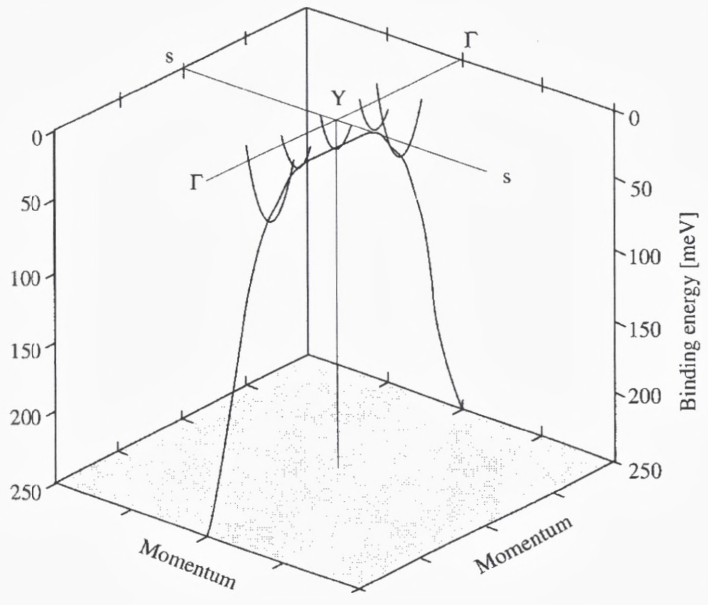

Figure 12. Three-dimensional representation of the extended saddle point in Y123. (Abrikosov et al., 1993).

the LDA calculated surface. This is a hole surface, despite the sign of the Hall coefficient. However, Lindroos and Bansil (1995) calculate that for some (0 0 1) surface terminations, there is a band of surface states which crosses the Fermi level which is easily confused with the bulk band crossing E_F. King et al., also determined a part of the Fermi surface for an overdoped sample ($x = 0.22$), and the hole surface was smaller, as expected for fewer holes. The effect of doping on surface states has yet to be examined. $Nd_{2-x}Ce_xCuO_4$ has an extended flat band, like those found in p-type cuprates, but it was much further, about 300 meV, below E_F.

6 Interpretation and summary

There are several microscopic models for the normal state of cuprates and several models for the formation of the superconducting state. ARUPS studies usually cannot so much as verify a model as eliminate one or more models, and place limits on surviving models. The theoretical literature is very large, and many photoelectron spectra have been calculated with several models. Almost all have

shown some agreement with experiment! Even the recent finding of a gap above T_c and the loss of part of the large Fermi surface have several possible explanations. Rather than try to explain all the accepted aspects of the ARUPS spectra in terms of each model, we list below the important features of such spectra that all models must account for. For the sake of brevity, we make the assumption that results found on one type of hole-doped cuprate, e.g., Bi2212, eventually will be found on the other n-type cuprates. This may not be true in detail, and perhaps not in one or more gross features.

1. For metallic cuprates, the Fermi surface is "large" and very close to that of the LDA calculations. Luttinger's theorem is valid. Correlation effects appear as an increased effective mass of the bands crossing the Fermi level. Detailed agreement with the LDA bands below the Fermi level has not yet been found. Some parts of predicted Fermi surfaces have not been found.

2. For underdoped, but still metallic, cuprates it appears that part of the large Fermi surface is lost.

3. There is an extended line of saddle critical points just below E_F, the position depending on which cuprate and on the doping level.

4. Below T_c a gap with $d_{x^2-y^2}$ symmetry, or something which effectively produces a symmetry of this form, appears. Its maximum magnitude is about 25 meV which occurs for a wave vector directed along the Cu–O bond. Above T_c a similar gap appears in underdoped samples.

5. There is a dip in the spectrum at about 90 meV below E_F that appears to correlate with the gap parameter Δ.

Recent theoretical work has tied together some of these features. The shadow bands were first predicted by Kampf and Schrieffer (1990), a result of coupling states $\mathbf{k}$ and $\mathbf{k} + \mathbf{Q}$ by antiferromagnetic fluctuations where $\mathbf{Q} = (\pi, \pi)$. The calculation required for observable shadow bands a magnetic correlation length considerably longer than that measured. Langer et al. (1996) were able to compute the self energy for a one-band, two-dimensional Hubbard model with realistic dispersion. The resultant spectral density exhibited both shadow bands and the "90 meV dip", while the correlation length was small. The calculated dependence of the Fermi surface on hole doping, and the energy and doping dependence of the quasiparticle lifetime were in qualitative agreement with experimental results.

Acknowledgements

The work reported herein has been carried out over seven years by a number of groups of changing composition. We acknowledge interesting conversations and the receipt of preprints from many individuals, including J.W. Allen, A.J. Arko, J.C. Campuzano, J. Fink, R. Liu, G. Margaritondo, M. Onellion, Z.X. Shen, M. Skibowski, T. Takahashi and B.W. Veal. The Ames Laboratory is operated by Iowa State University for the U.S. DOE under contract No. 7405-ENG-82.

The late Professor A.R. Mackintosh played a role in this work, for we have discussed, much to our benefit, this and other research work with him over the years.

References

Abrikosov AA, Campuzano JC and Gofron K, 1993: Physica C **214**, 73

Aebi P, Osterwalder J, Schwaller P, Schlapbach L, Shimoda M, Mochiku T and Kadowaki K, 1994: Phys. Rev. Lett. **72**, 2757

Aebi P, Osterwalder J, Schwaller P, Berger H, Beeli C and Schlapbach L, 1995: J. Phys. Chem. Solids **56**, 1845

Anderson RO, Claessen R, Allen JW, Olson CG, Janowitz C, Liu LZ, Park JH, Maple MB, Dalichaouch Y, de Andrade MC, Jardim RF, Early EA, Oh SJ and Ellis WP. 1993: Phys. Rev. Lett. **70**, 3163

Bansil A, Lindroos M, Gofron K, Campuzano JC, Ding H, Liu R and Veal BW, 1992: J. Phys. Chem. Solids **53**, 1541

Behner H, Rauch W and Gornik E, 1992: Appl. Phys. Lett. **61**, 1465

Bozovic I and van der Marel D, 1996: *Spectroscopic Studies of Superconductors* (SPIE, Bellingham)

Brenig W, 1995: Phys. Repts. **251**, 153

Calandra C and Manghi F, 1992: Phys. Rev. B **46**, 3600

Calandra C and Manghi F, 1994: J. Electron Spectrosc. Relat. Phenom. **66**, 453

Campuzano JC, Ding H, Norman MR, Randeria M, Bellman AF, Yokoya T, Takahashi Y, Katayama-Yoshida H, Mochiku T and Kadowaki K, 1996: Phys. Rev. B **53**, R14737

Cardona M and Ley L, eds., 1978: *Photoemission in Solids* (Springer Verlag, Berlin) Vol. 1

Coffey L and Coffey D, 1993: Phys. Rev. B **48**, 4184

Courths R and Hüfner S, 1984: Phys. Repts. **112**, 53

Dessau DS, Wells BO, Shen ZX, Spicer WE, Arko AJ, List RS, Mitzi DB and Kapitulnik A, 1991: Phys. Rev. Lett. **66**, 2160

Dessau DS, Shen ZX, Wells BO, King DM, Spicer WE, Arko AJ, Lombardo LW, Mitzi DB and Kapitulnik A, 1992: Phys. Rev. B **45**, 5095

Dessau DS, Shen ZX, King DM, Marshall DS, Lombardo LW, Dickinson PH, DiCarlo , Park CH, Loeser AG, Kapitulnik A and Spicer WE: 1993, Phys. Rev. Lett. **71**, 2781

Ding H, Bellman AF, Campuzano JC, Randeria M, Norman MR, Yokoya T, Takahashi T, Katayama-Yoshida H, Mochiku Y, Kadowaki K, Jennings G and Brivio GP: 1996a, Phys. Rev. Lett. **76**, 1533

Ding H, Yokoya T, Campuzano JC, Takahashi T, Randeria M, Norman MR, Mochiku T, Kadowaki K and Giapintzakis J: 1996b, Nature **382**, 51

Edwards HL, Markert JT and de Lozanne AL, 1992: Phys. Rev. Lett. **69**, 2967
Emery VJ and Kivelson SA, 1995: Nature **374**, 434
Fehrenbacher R, 1996: preprint (submitted to Phys. Rev. B)
Fink J, Nücker N, Pellegrin E, Romberg H, Alexander M and Knupfer M: 1994, J. Electron Spectrosc. Rel. Phenom. **66**, 395
Gofron K, Campuzano JC, Abrikosov AA, Lindroos M, Bansil A, Ding H, Koelling D and Dabrowski B, 1994: Phys. Rev. Lett. **73**, 3302
Hüfner S, 1994: Adv. Phys. **43**, 183
Hüfner S, 1995: *Photoelectron Spectroscopy* (Springer Verlag, Berlin)
Kampf AP and Schrieffer JR, 1990: Phys. Rev. B **42**, 7967
Kelley RJ, Ma J, Onellion M, Marsi M, Almeras P, Berger H and Margaritondo G, 1993: Phys. Rev. B **48**, 3534
Kevan SD, 1986: Phys. Rev. B **33**, 4364
Kevan SD, ed., 1992: *Angle-resolved Photoemission – Theory and Current Applications* (Elsevier Science Publishers, Amsterdam)
King DM, Shen ZX, Dessau DS, Wells BO, Spicer WE, Arko AJ, Marshall DS, DiCarlo J, Loeser AG, Park CH, Ratner ER, Peng JL, Li ZY and Greene RL, 1993: Phys. Rev. Lett. **70**, 3159
Langer M, Schmalian J, Grabowski S and Bennemann KH, 1996: Phys. Rev. Lett. **75**, 4508
Ley L and Cardona M, eds., 1979: *Photoemission in Solids* (Springer Verlag, Berlin) Vol. 2
Liechtenstein AI, Gunnarsson O, Andersen OK and Martin RM, 1996: preprint (submitted to Phys. Rev. B)
Lindberg PAP, Shen ZX, Spicer WE and Lindau I, 1990: Surface Science Reports **11**, 1
List RS, Arko AJ, Fisk Z, Cheong SW, Conradson SD, Thompson JD, Pierce CB, Peterson DE, Bartlett RJ, Shinn ND, Schirber JE, Veal BW, Paulikas AP and Campuzano JC, 1988: Phys. Rev. B **38**, 11966
Lindroos M and Bansil A, 1995: Phys. Rev. Lett. **75**, 1182
Liu R, Veal BW, Paulikas AP, Downey JW, Kostic PJ, Fleshler S, Welp U, Olson CG, Wu X, Arko AJ and Joyce JJ, 1992: Phys. Rev. B **46**, 11056
Loeser AG, Shen ZX, Dessau DS, Marshall DS, Park CH, Fournier P and Kapitulnik A, 1996: Science **273**, 325
Lynch DW and Olson CG, 1997: *Photoemission of High-Temperature Superconductors* (to be published)
Ma J, Quitmann C, Kelley RJ, Berger H, Margaritondo G and Onellion M, 1995: Science **267**, 862
Marshall DS, Dessau DS, Loeser AG, Park CH, Matsuura AY, Eckstein JN, Bozovic I, Fournier P, Kapitulnik A, Spicer WE and Shen ZX, 1996: Phys. Rev. Lett. **76**, 4841
Massida S, Yu J and Freeman AJ, 1988: Physica C **152**, 251
Olson CG, Liu R, Yang AB, Lynch DW, Arko AJ, List RS, Veal BW, Chang YC, Jiang PZ and Paulikas AP, 1989: Science **245**, 731
Olson CG, Liu R, Lynch DW, List RS, Arko AJ, Veal BW, Chang YC, Jiang PZ and Paulikas AP, 1990: Phys. Rev. B **42**, 381
Osterwalder J, Aebi P, Schwaller P, Schlapbach L, Shimoda M, Mochiku T and Kadowski K, 1995: Appl. Phys. A **60**, 247
Plummer EW and Eberhardt W, 1982: in *Advances in Chemical Physics*, eds. I. Prigogine and S.A. Rice (John Wiley and Sons, New York) Vol. XLIV, p. 533
Randeria M, Ding H, Campuzano JC, Bellman AF, Jennings G, Yokoya T, Takahashi T, Katayama-Yoshida H, Mochiku T and Kadowaki K, 1995: Phys. Rev. Lett. **74**, 4951
Sakisaka Y, Maruyama T, Morikawa Y, Kato H, Edamoto K, Okusawa M, Aiura T, Yanashima H, Terashima T, Bando Y, Iijima K, Yamamoto K and Hirata K, 1990: Phys. Rev. B **42**, 4189

Schroeder N, Böttner R, Ratz S, Dietz E, Gerhardt U and Wolf T, 1993: Phys. Rev. B **47**, 5287
Shen ZX and Dessau DS, 1995: Phys. Repts. **253**, 1
Shen ZX, Dessau DS, Wells BO, King DM, Spicer WE, Arko AJ, Marshall D, Lombardo LW, Kapitulnik A, Dickinson P, Doniach S, DiCarlo J, Loese, AG and Park CH, 1993: Phys. Rev. Lett. **70**, 1553
Shen ZX, Spicer WE, King DM, Dessau DS and Wells BO, 1995: Science **267**, 343
Singh DJ and Pickett WE, 1995: Phys. Rev. B **51**, 3128
Smith NV and Himpsel FJ, 1982: in *Handbook of Synchrotron Radiation*, eds. D.E. Eastman, Y. Farge and E.-E. Koch (North-Holland Publishing Co., Amsterdam) Vol. I b, chapt. 9
Smith NV, Thiry P and Petroff Y, 1993: Phys. Rev. B **47**, 15476
Tobin JG, Olson CG, Gu C, Liu JZ, Solal FR, Fluss MJ, Howell RJ, O'Brien JC, Radousky HB and Sterne PA, 1992: Phys. Rev. B **45**, 5563
Varma CM and Littlewood PB, 1992: Phys. Rev. B **46**, 405
Veal BW and Gu C, 1994: J. Electron Spectrosc. Relat. Phenom. **66**, 321
Wells BO, Shen ZX, Dessau DS, Spicer WE, Mitzi DB, Lombardo LW, Kapitulnik A and Arko AJ, 1992: Phys. Rev. B **46**, 11830
Yokoya T, Takahashi T, Mochiku T and Kadowaki K, 1996: Phys. Rev. B **53**, 14055